Chemical Engineering Journal 101 (2004) 367–372

Chemical Engineering Journal

www.elsevier.com/locate/cej

Interface configuration of the two layered laminar flow in a curved microchannel

Yoshiko Yamaguchi [a], Fuminori Takagi [c], Takanori Watari [c], Kenichi Yamashita [a], Hiroyuki Nakamura [a], Hazime Shimizu [a], Hideaki Maeda [a,b,*]

[a] *Micro-space Chemistry Laboratory, National Institute of Advanced Industrial Science and Technology, 807-1, Shuku-machi, Tosu 841-0052, Japan*
[b] *Graduate School of Engineering Sciences, Kyushu University, Japan*
[c] *Graduate School of Science and Engineering, Saga University, Japan*

Received 31 July 2003; accepted 28 October 2003

Abstract

Three-dimensional direct observation of fluid dynamics in microchannels was performed by confocal fluorescence microscopy and three-dimensional computational fluid dynamics simulation to examine the fluid interface in curved microchannels. Results revealed that the interface of the two laminar flows is heavily distorted and increases the interfacial area because of its curved structure. The combined effect of flow velocity, curvature radius of the microchannel, density, and viscosity on the interface configuration was simulated. Increasing flow velocity and density complicated the interface configuration more. In contrast, increasing curvature radius and viscosity simplified it. Interface distortion is emphasized in a microchannel whose depth is five times its width. The interface configuration is important because it affects diffusion and chemical reactions that occur at the interface. Results herein emphasize the importance of microchannel design based on a three-dimensional comprehension of fluids and their associated mixing behavior.

Keywords: Microfluidics; Microreactor; Computational fluid dynamics; Laminar flow

1. Introduction

Miniaturized devices referred to as microreactors produce special and remarkable chemical reaction behavior, such as high-conversion synthesis of organic compounds [1], extremely rapid yield of enzyme reaction [2–4], and so on. Mixture of fluids in a microchannel is strongly restricted to molecular diffusion through the interface of miscible solutions because the laminar flow is maintained in a microchannel because of such flows' low Reynolds number. Therefore, interfaces between liquid/liquid phases in microchannels and control of those interfaces are anticipated to play an important role in chemical reactions in the microreactor. They may also aid in elucidating the mechanism for acceleration of enzyme reactions. Nevertheless, few reports have addressed fluid dynamics in a microchannel.

This work is intended to compare results of computational fluid dynamics (CFD) simulation and observation of fluid dynamics in a three-dimensional manner. Thereafter, this study estimates effects of density, viscosity, and so on. Fluidic simulation and visualization have been performed extensively at the macro-level and the secondary flow induced in curved rectangular channels has been analyzed [5,6]. However, at the micro-level, research on three-dimensional flow visualization has begun only recently. Wang et al. [7] used small beads as tracers, but these beads presented the possibility of disturbing the flow in the microspace. Manz et al. [8] measured velocity distribution in a capillary using a nuclear magnetic resonance (NMR) microimaging technique, but that spatial resolution was greater than 10 μm, which was not sufficiently fine for microchannel measurements. On the other hand, a measurement technique using single molecule fluorescein coupled with fluorescence confocal microscopy was recently developed; it permitted a description of flow with spatial resolution as high as 1 μm [9,10]. This principle was applied in that study to observe interface configurations of micro-fluids in a microchannel. An understanding of flow dynamics would be desirable for designing chemical reactions at the solution interface [11,12], as well as extraction between aqueous and organic phases [1]. Moreover, it would aid in elucidating the origin of much higher chemical reaction yields in microchannel reactors, compared to those in well-mixed batch reactors [2–4].

* Corresponding author. Tel.: +81-942-81-3676; fax: +81-942-81-3657.
E-mail address: maeda-h@aist.go.jp (H. Maeda).

1385-8947/$ – see front matter © 2004 Elsevier B.V. All rights reserved.
doi:10.1016/j.cej.2003.10.018

2. Experimental

A microchannel was fabricated mechanically on a 3 mm × 7 mm PMMA plate, using a Robodrill (Fanuc, Ltd., Japan) with a flat end mill (Ø200 μm) [13]. Fig. 1 shows the design of the microchannel used in these experiments: 20 mm straight channels (width and depth were 200 μm for each) were connected with semicircle channels whose curvature radii were 500 μm. Laser microscope measurement determined the basal wall roughness to be less than 5% of the depth. After fabrication, the channel plate was covered with a flat top plate and sealed by heating. Programmable syringe pumps (KD Scientific Inc., USA) were connected to the inlets with Teflon tubing.

Two liquids were prepared: purified water and fluorescein (>95%, Wako Pure Chemical Industries, Ltd., Japan) 50 μmol/l solution. These two liquids were injected from the left and right microchannel inlets. These liquids were merged to form a side-by-side parallel flow in the straight channel. Confocal fluorescence microscopy system (Nikon Corp., Japan) was used for measurement of the interface of the water and fluorescein solution in a three-dimensional manner. The wavelength and output of the Ar laser were 488 nm and 25 mW, respectively.

Three-dimensional computational fluid dynamics simulations were performed using Fluent 6.0 (Fluent Inc., USA) based on a finite-volume method. Although the mixing model for miscible solutions was adopted for calculation, the diffusion coefficient was set to zero to clear the configuration of the interface between solutions. The effect of interaction of the wall and liquid becomes obvious at the micro-level. In fact, molecules of the liquid are reported to slip on the channel wall microscopically [14,15]. However, the present study assumes a no-slip condition for simplicity [16].

The microchannel was assumed to be identical to the design described above. The cross-sectional plane of the microchannel was divided in 40 mesh × 40 mesh cells; the total number of mesh cells in the calculated space was about 500,000. Circular arcs at the curves were divided in 120 mesh cells, and each of the straight parts was divided in 24 mesh cells. The mesh sizes near the curves were about 10 μm and were lengthened toward the center of the straight parts in incremental steps. An iterative calculation for solving Navier–Stokes equations was carried out with second-order accuracy for pressure; the SIMPLE algorithm was used for pressure–velocity coupling. Iterative calculation was terminated using the criterion that the error of the equation of continuity is less than 1.0E−9 compared with that at the start of calculation. The liquid was set to be purified water (density and viscosity were 1.0E+3 $kg\,m^{-3}$ and 1.0E−3 $kg\,m^{-1}\,s^{-1}$, respectively).

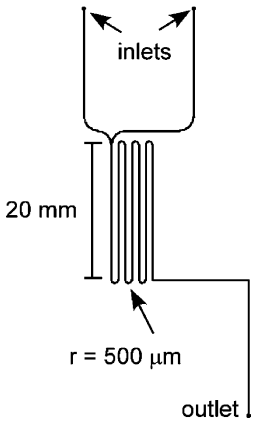

Fig. 1. Design of a microchannel. The top view is shown.

3. Results and discussion

Fig. 2 shows simulation and observation results for fluidic behavior at the average velocity of 25 mm/s (the Reynolds number, $Re \sim 5$) and 125 mm/s ($Re \sim 25$). Characters a, b, and c in the figure correspond to situations before the first turn, after the first turn, and after the second turn. In the simulation where the average velocity was 25 mm/s, the inner liquid was thrust outward by inertial force. Consequently, the vertical line that crossed the central axis was distorted after passing the first curve. Inertial force was exerted in the opposite direction at the second curve; thereupon, the distorted line returned almost to the initial vertical line. However, the vertical line that was distorted at the first curve did not recover to the initial vertical line after the second curve when the average velocity was 125 mm/s. The interface between the two liquids was permanently wave-shaped. The observation results are shown beside the respective simulation results. The fluorescein solution, which initially flows on the right-hand side in this cross-section, is thrust outwards after the first turn. It then returns to the initial position after the second turn at the average velocity of 25 mm/s. When the average velocity was 125 mm/s, the Ω-shaped line of the boundary was observed clearly after the first curve. The M-shaped line of the boundary was also observed after the second curve. Experimental data agreed well with the simulation data in terms of general trend. Lengths of arrows (i) and (ii) in Fig. 2 were measured for a detailed comparison. Arrows (i) and (ii) are at positions of 33 and 100 μm from the top wall, respectively. Table 1 shows percentages of these lengths to the channel width. Although most results show good agreement between the simulation and observation, the values differ in results of (b) at the average velocity of 25 mm/s. A computation with nearly double the number of mesh cells was carried out to validate the simulation. This computation produced no difference from the above values. Several reasons for error in observation can be considered such as pulsation of the syringe pumps, noise in detection of fluorescence using the confocal fluorescence microscopy, distortion of optical system through PMMA plates, and so on. The difference mentioned above might be caused by integrative error engendered by them. However, there remains

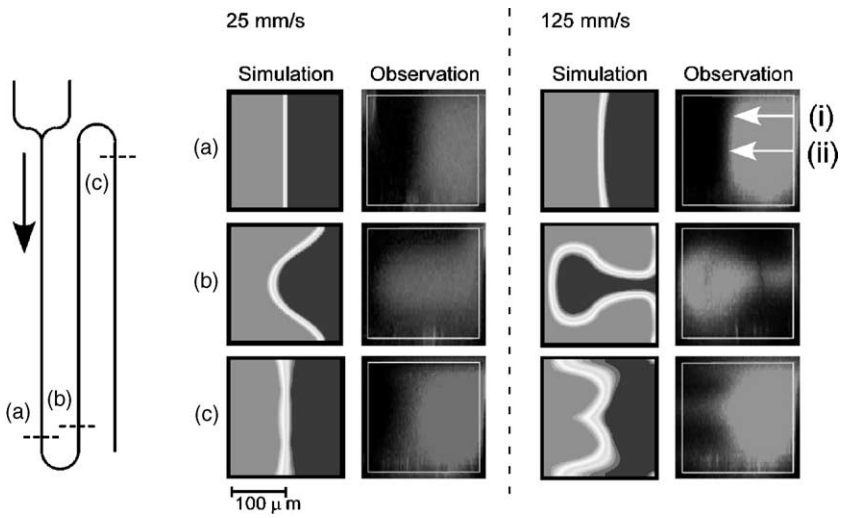

Fig. 2. Comparison of simulation and observation experiment results for three-dimensional flow patterns. Initially vertical lines are distorted during passage through the microchannel. Average velocity = 25 and 125 mm/s.

the possibility that it might result from different hydrophilicities of the wall for simulation and observation. It is necessary to be examined in more depth.

Fig. 3 shows path lines of the fluid on the vertical line. Path lines produce a pair of vortices in the cross-sectional plane of the microchannel, as shown notably at the average velocity of 125 mm/s. These vortices are known as the Dean vortices. The secondary flow causes deformations of the interface mentioned above. The secondary flow in a curved channel is expressed by the Dean number,

$$K = Re\sqrt{\frac{a}{R}}, \quad (1)$$

where Re is the Reynolds number, a the channel radius, and R the curvature radius. A single vortex pair appears in the region of $K < 140$ [6]. The value of the Dean number in the present study is less than 20 and fulfilled $K < 140$, which indicates that a single vortex pair of the secondary flow appears at the corner of the microchannel in this study. It is generally known that the velocity along the central axis in a rectangle channel is the greatest among those in the cross-sectional plane.

Table 1
Quantitative comparison of simulation and observation experiment results in Fig. 2[a]

		25 mm/s		125 mm/s	
		Simulation	Observation	Simulation	Observation
(a)	(i)	51	45	47	55
	(ii)	51	47	48	58
(b)	(i)	33	18	65	72
	(ii)	62	83	88	96
(c)	(i)	51	55	45	55
	(ii)	51	61	53	66

[a] Rows (a), (b), (c), (i), (ii) correspond to those in Fig. 2. Values are the percentages of lengths of the arrows in Fig. 2.

Therefore, the flow near the central axis is the most strongly affected by the inertial force. The liquid at the center is forced outward; consequently, the liquid at the upper and lower periphery moves inward to compensate for the outward flow. The inner fluid thrusts more outward in the higher speed fluid because the inertial force is exerted more strongly. Distortion of the interface recovers toward the original vertical plane by the secondary flow in the opposite direction at the second curve. However, this recovery is incomplete, as shown in Fig. 3, because the strength of the secondary flow is smaller at the periphery than the channel center. This incomplete recovery perturbs the boundary line from the straight one, especially at high velocity. In a case where the Reynolds number and the Dean number are much smaller than the values which are addressed in this work, the interfacial distortion must be negligible because the inertial forces are small. In a case where the Reynolds and

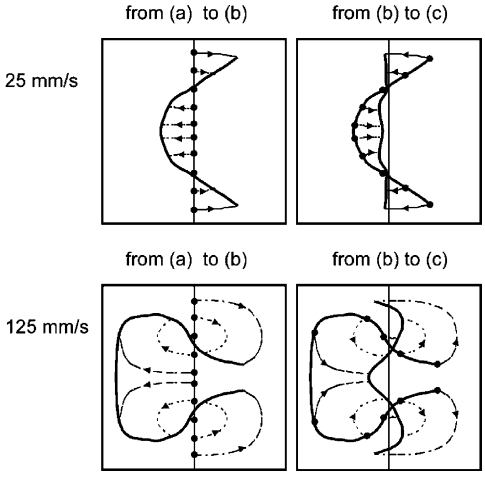

Fig. 3. Pass line of the fluid on the vertical lines.

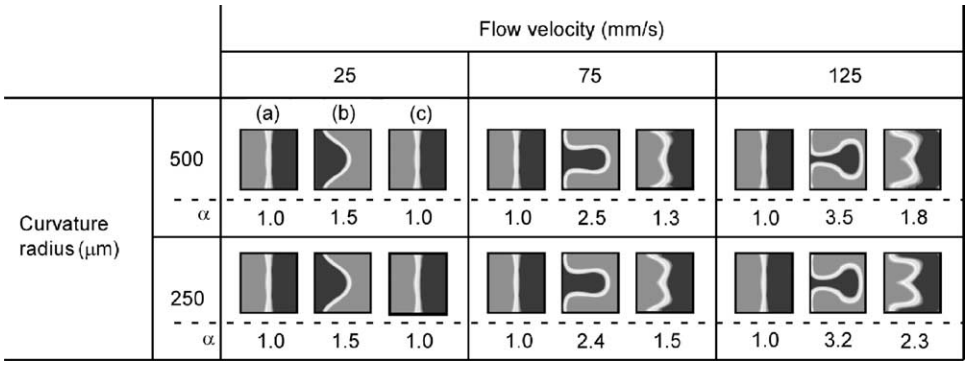

Fig. 4. Effects of curvature radius and average velocity on flow patterns and interface configurations in the microchannel. α means the ratio of the interface area to the flat interface area. Points (a), (b), and (c) correspond to positions in the microchannel shown in Fig. 4.

Dean numbers are much larger, the interface configuration might be more complicated because the secondary flow is complicated [6]. However, it would be difficult to achieve such large Reynolds and Dean numbers in microchannels because of the high pressure-drop.

Fig. 4 summarizes interface configurations as functions of average velocity and curvature radius. Data for curves with a curvature radius of 250 μm are included in this figure. Distortion of the interface is stronger at the 250 μm curvature radius than at 500 μm because the smaller curvature radius increases the inertial force.

Fig. 4 also shows the increasing rate of the length of boundary through which diffusion occurs. The length of the boundary increases to αL_0, where L_0 is the length of boundary when the boundary is a vertical straight line (that is, the interfacial plane is simple and flat), and α ($=L/L_0$) is a coefficient larger than unity. The lengths L and L_0 were computed approximately using 40 mesh × 40 mesh cells in the cross-sectional plane after each curve in the simulation results. Thus, value α in Fig. 5 indicates the ratio of the interface areas in the straight part of the channel, which occupies most of the channel. The value of α reaches more than three at an average velocity of 125 mm/s.

Liquid phase chemical reactions and material syntheses in three-dimensional microspaces are influenced greatly by diffusion across the interface. The time necessary for diffusion is expressed as $t_d = s^2/D$ (characteristic diffusion time), where D is the diffusion coefficient and s is the thickness of the fluid layers. This expression is inferred from the equation $D \sim \langle x^2 \rangle / t$, where x is the moving distance. The amount of interfacial area per unit volume a is called the intermaterial area density; it has the relation $s \approx 1/a$. The amount of a is expressed as $a \approx L/S$ where L is the length of boundary through which diffusion occurs and S is the mixing area [17]. Characteristic diffusion time t_d is proportional to s^2, indicating that the time required for diffusion decreases with an increase in $L^2 = (\alpha L_0)^2$. As shown in Fig. 5, α exceeds three in some cases. This fact suggests that the diffusion rate through the interface of the two liquids in microchannels with curves greatly increases in comparison to that in straight microchannels. The interface of the liquids disappears after passing a certain number of curves in reality because the two liquids used in this study are miscible. In some cases, reaction rates may be affected strongly by the manner in which microchannels receive and mix aqueous solutions.

Fig. 5 summarizes interface configurations as functions of density and viscosity. It is difficult to execute observation experiments using liquids with greatly different density and viscosity ratios. Simulation results, however, suggest that a high density ratio between fluids emphasizes distortion of the interface; a high viscosity ratio moderates it.

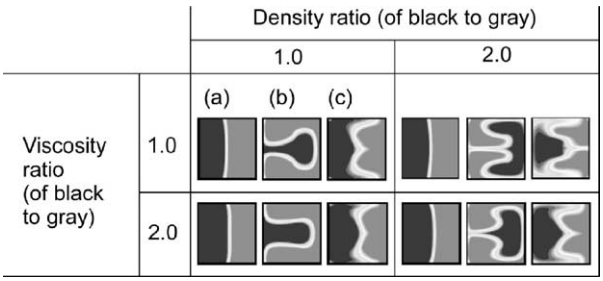

Fig. 5. Effects of density and viscosity on flow patterns and interface configurations in the microchannel. Average velocity was 125 mm/s.

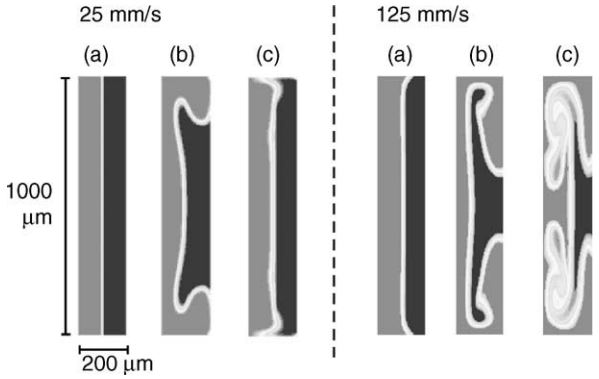

Fig. 6. Simulated distortion of the initially vertical line during its passage through the microchannel. The width and depth are 200 and 1000 μm, respectively.

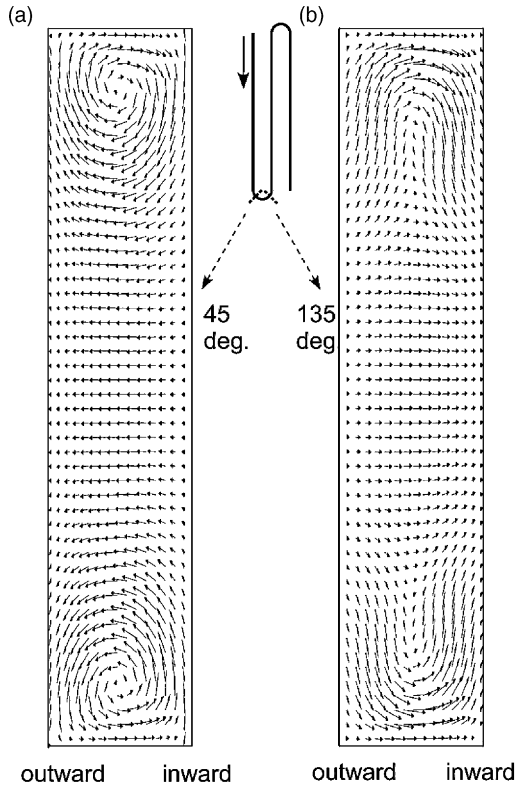

Fig. 7. Velocity distribution of the secondary flow at the curve, which yields a complicated interface configuration shown in Fig. 6. Arrow lengths indicate the velocity magnitude in the cross-sectional plane.

Fig. 6 shows the complicated interface configuration of a microchannel whose aspect ratio is 5. Although average velocities and curvature radius are the same as those in Figs. 2 and 3, interface distortion is stronger than the rectangle channels. Fig. 7 shows the secondary flow at the average velocity of 125 mm/s. In channels whose aspect ratio is high, a vortex pair of the secondary flow appears near to the top and bottom walls, and not in the middle of the channel (Fig. 7a). The vortex pair, however, begins to collapse near the end of the curve (Fig. 7b). These features of vortices engender the extremely complex configuration of the interface.

4. Conclusions

Three-dimensional computational fluid dynamics simulations were performed regarding fluidic behavior of laminar liquid flows in microchannels with curves. Simulation results were validated by three-dimensional observation through confocal fluorescence microscopy. These results revealed that the interface configuration of two liquids was affected by secondary flow, induced by inertial force at the corners. The flow velocity, density, viscosity, curvature radius, and aspect ratio of the cross-sectional plane of the channel affect the interface configuration. Increasing flow velocity and density complicated the interface configuration more. In contrast, increasing curvature radius and viscosity simplified it. Interface distortion is emphasized in a microchannel whose depth is five times its width. The increased interface area of two laminar liquids could promote a mass transfer based on diffusion. Success of chemical reactions and material syntheses inside microchannels often depends on flow properties: higher yields are thereby obtained than by reactions in well-mixed reactors. On the other hand, some kinds of chemical reactions that require a stable interface exist, e.g., extraction of materials and separation of solvents. In such cases, the microchannel structure should be considered in the context of minimizing effects of the secondary flow. Results obtained in this study suggest the importance of microchannel design based on a three-dimensional comprehension of the fluid and accompanying mixing behavior.

Acknowledgements

The authors greatly appreciate Professor S. Morooka at Fukuoka University, Associate Professor K. Kusakabe, and Research Associate K. Sotowa at Kyushu University, for suggestions and discussion for the computational fluid dynamics simulation.

References

[1] H. Hisamoto, T. Saito, M. Tokeshi, A. Hibara, T. Kitamori, Fast and high conversion phase-transfer synthesis exploiting the liquid–liquid interface formed in a microchannel chip, Chem. Commun. (2001) 2662–2663.
[2] M. Miyazaki, H. Nakamura, H. Maeda, Improved yield of enzyme reaction in microchannel reactor, Chem. Lett. (2001) 442–443.
[3] Y. Tanaka, M.N. Slyadnev, K. Sato, M. Tokeshi, H.-B. Kim, T. Kitamori, Acceleration of an enzymatic reaction in a microchip, Anal. Sci. 17 (2001) 809–810.
[4] K. Kanno, H. Maeda, S. Izumo, M. Ikuno, K. Takeshita, A. Tashiro, M. Fujii, Rapid enzymatic transglycosylation and oligosaccharide synthesis in a microchip reactor, Lab on a Chip 2 (1) (2002) 15–18.
[5] K.C. Cheng, R.-C. Lin, J.-W. Ou, Fully developed laminar flow in curved rectangular channels, Trans. ASME, Ser. I 98 (1) (1976) 41–48.
[6] K.N. Ghia, J.S. Sokhey, Laminar incompressible viscous flow in curved ducts of regular cross-sections, Trans. ASME, Ser. I 99 (4) (1977) 640–648.
[7] W. Wang, Y. Liu, G.J. Sonek, M.W. Berns, R.A. Keller, Optical trapping and fluorescence detection in laminar flow streams, Appl. Phys. Lett. 67 (8) (1995) 1057–1059.
[8] B. Manz, P. Stilbs, B. Jonsson, O. Soderman, P.T. Callaghan, NMR imaging of the time evolution of electroosmotic flow in a capillary, J. Phys. Chem. 99 (29) (1995) 11297–11301.
[9] M. Gosch, H. Blom, J. Holm, T. Heino, R. Rigler, Hydrodynamic flow profiling in microchannel structures by single molecule fluorescence correlation spectroscopy, Anal. Chem. 72 (2000) 3260–3265.
[10] R.F. Ismagilov, G.M. Whitesides, Experimental and theoretical scaling laws for transverse diffusive broadening in two-phase laminar flows in microchannels, Appl. Phys. Lett. 76 (17) (2000) 2376–2378.
[11] P.J.A. Kenis, R.F. Ismagilov, G.M. Whitesides, Microfabrication inside capillaries using multiphase laminar flow patterning, Science 285 (1999) 83–85.

[12] B. Zhao, N.O.L. Viernes, J.S. Moore, D.J. Beebe, Control and applications of immiscible liquids in microchannels, J. Am. Chem. Soc. 124 (2002) 5284–5285.
[13] H. Kawazumi, A. Tashiro, K. Ogino, H. Maeda, Observation of fluidic behavior in a polymethacrylated microchannel by a simple spectroscopic analysis, Lab on a Chip 1 (2002) 8–10.
[14] P.A. Thompson, S.M. Trolan, A general boundary condition for liquid flow at solid surfaces, Lett. Nature 389 (1997) 360–362.
[15] J.-L. Barrat, L. Bocquet, Influence of wetting properties on hydrodynamic boundary conditions at a fluid/solid interface, Faraday Discuss. 112 (1999) 119–127.
[16] A.D. Stroock, S.K. Dertinger, G.M. Whitesides, A. Ajdari, Patterning flows using grooved surfaces, Anal. Chem. 74 (2002) 5306–5312.
[17] J.M. Ottino, The Kinematics of Mixing: Stretching, Chaos, and Transport, Cambridge University Press, Cambridge, 1989.